PHYSICS

Scanning wave photopolymerization enables dye-free alignment patterning of liquid crystals

Kyohei Hisano,[1] Miho Aizawa,[1] Masaki Ishizu,[1] Yosuke Kurata,[1] Wataru Nakano,[1] Norihisa Akamatsu,[1] Christopher J. Barrett,[1,2] Atsushi Shishido[1,3]*

Hierarchical control of two-dimensional (2D) molecular alignment patterns over large areas is essential for designing high-functional organic materials and devices. However, even by the most powerful current methods, dye molecules that discolor and destabilize the materials need to be doped in, complicating the process. We present a dye-free alignment patterning technique, based on a scanning wave photopolymerization (SWaP) concept, that achieves a spatial light–triggered mass flow to direct molecular order using scanning light to propagate the wavefront. This enables one to generate macroscopic, arbitrary 2D alignment patterns in a wide variety of optically transparent polymer films from various polymerizable mesogens with sufficiently high birefringence (>0.1) merely by single-step photopolymerization, without alignment layers or polarized light sources. A set of 150,000 arrays of a radial alignment pattern with a size of 27.4 μm × 27.4 μm were successfully inscribed by SWaP, in which each individual pattern is smaller by a factor of 10^4 than that achievable by conventional photoalignment methods. This dye-free inscription of microscopic, complex alignment patterns over large areas provides a new pathway for designing higher-performance optical and mechanical devices.

INTRODUCTION

The ability to macroscopically align liquid crystal (LC) films to controlled hierarchical alignment is key for the development of next-generation high-performance electronic, photonic, mechanical, and biomedical organic devices (*1*–*5*). Current methods achieve this control of large-area alignment of LCs, having intrinsic structural ordering over various length scales from nanometer to micrometer (*6*–*9*), by applying uniform external fields along one direction, such as mechanical stress, surface rubbing treatment, and electromagnetic or light fields (*10*–*12*). Of these techniques, mechanical stress is the most simple and most powerful method when only one-dimensional (1D) alignment of molecules is required, yet the other options offer a possibility for hierarchical alignment over two dimensions. Among these more advanced 2D techniques, light-driven alignment control (photoalignment) provides perhaps the greatest potential for fine control over molecular orientation, because of its remote and precise influence, and suitability for micro- or nanofabrication, which can enable many applications that require more complex alignment patterns (*13*–*19*). With conventional photoalignment methods, one typically irradiates an LC film containing added photoresponsive (dye) molecules with spatiotemporally uniform polarized light and controls the net LC alignment via the interaction between the dye dipole and the polarization axis of light (Fig. 1A). In addition to low–molecular weight LC systems containing photoreactive dyes, polymer systems, such as side-chain LC polymers, supramolecules, surface-grafted polymers, and block copolymers, have been explored (*11*–*13*, *20*–*30*). However, a fundamental drawback of all these systems is that strong dyes that photoisomerize, photocrosslink, photorearrange, or photodecompose are always required to be added, which can discolor or degrade optical or stability properties. A dye-free system is thus highly desirable, and so far, two approaches have been explored. One is a two-step alignment method; LC materials, coated over a very thin dye-containing photoalignment layer, are aligned and, in some cases, fixed by a subsequent polymerization. This method demonstrates the impressive success of top-down approaches in achieving stimuli-responsive 2D aligned LCs and elastomers used in photonics, solar energy harvesting, microfluidics, and soft-robotics devices (*2*, *31*–*33*). However, it is time-consuming, costly, or even impossible to create a film having macroscopic arrays of microalignment patterns, because the patterning requires a precise and dynamic control of the polarization direction of incident light in each pixel in desired patterns. The pixel size to inscribe the patterns is governed by the focused spot size of the light used and thus is limited to tens of square micrometers, resulting in a pattern with a size of square millimeters. The other approach uses surface topography to circumvent the abovementioned critical limitations of conventional photoalignment, a highly desired and valuable engineering goal. In particular, LCs can be aligned over a surface topography template by lithography, nanoimprinting, ink-jet printing, etc. (*12*, *34*–*37*). However, even with these advanced methods that enable 2D micropatterning of molecular alignment versatilely and quickly, these methods still require multiprocessing steps for fabricating these templates, resulting in a time-consuming and costly overall process, and they also have difficulty in fabricating thin films because of their surface roughness arising from the topographies of the templates.

We report here the development of a new concept of scanning wave photopolymerization (SWaP) using spatiotemporal scanning of focused guided light, triggering a mass flow in the film as the polymerization reaction propagates, which then results in LC alignment coincident with the incident light patterns (Fig. 1B). A desired target pattern of molecular alignment is thus achieved in a single step by light-triggered mass flow, where arbitrary spatiotemporal scanning patterns of the incident light propagate as a wavefront of controlled flow. This new technique is able to generate arbitrary alignment patterns with fine control over large areas, in a wide variety of photopolymerizable LC materials, without the need for any added dyes or pre- or subsequent processing steps. As a further advantage over other current techniques, the size of the final alignment patterns would be, in principle, restricted only by light diffraction limits, and complexity of any patterns in 2D is then effectively unlimited. Previously, we had serendipitously found a key

[1]Laboratory for Chemistry and Life Science, Institute of Innovative Research, Tokyo Institute of Technology, 4259 Nagatsuta, Midori-ku, Yokohama 226-8503, Japan. [2]Department of Chemistry, McGill University, Montreal, Quebec, Canada. [3]Precursory Research for Embryonic Science and Technology, Japan Science and Technology Agency, 4-1-8 Honcho, Kawaguchi 332-0012, Japan.
*Corresponding author. Email: ashishid@res.titech.ac.jp

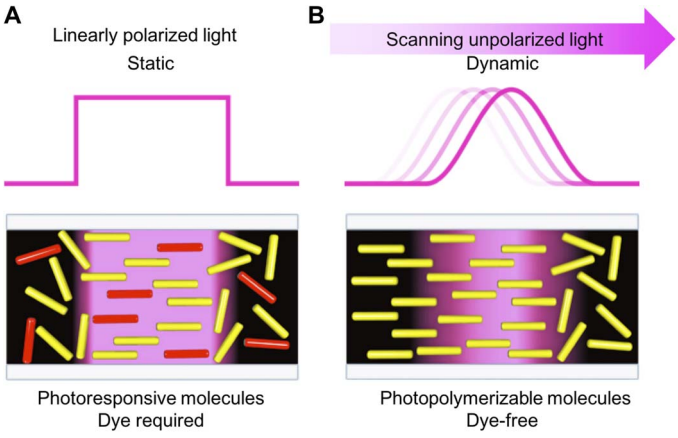

Fig. 1. Schematic representations of photoirradiation for controlling molecular alignment. (**A**) Conventional photoalignment method via the interaction between linearly polarized light and photoresponsive dye molecules (red rod) and simultaneous cooperative effect to align LCs (yellow rod), where light is spatiotemporally uniform. (**B**) New concept proposed here for generating molecular alignment merely by photopolymerization with spatiotemporal scanning of light patterns, termed "SWaP." Pink and black regions represent irradiated and unirradiated regions, respectively.

related effect that leads to the development of the present SWaP concept, where photopolymerization through a spatially patterned photomask led to an unexpected molecular alignment at the pattern edges (*38*), and this unusual driving force was suspected to be a mass flow of molecular diffusion in a light intensity gradient (*39*–*43*). This was an exciting initial discovery with potential for development; however, the detailed mechanism of the underlying process was unclear, and using masks limited the size of alignment achievable to a scale of hundreds of micrometers and constrained the variety of alignment patterns possible to those of preformed masks available. Using masks also limited pattern inscription necessarily to only a serial process, and not to parallel fabrication. Thus, to develop SWaP, we used the gradient light technique as a base to control macroscopic molecular alignment, but transitioned from large preformed masks to mask-free scanning light, to expand the capability to arbitrary 2D patterns that could be patterned quickly and, in parallel, contact-free, and in a resolution down to the diffraction limit of the light used. As a first transition step, and for ease of characterization, we began by aligning a dye-free LC polymer film simply by 1D scanning of a slit of light during photopolymerization. The resultant film had macroscopic, in-plane, 1D molecular alignment along the light scanning direction. This macroscopic alignment was successfully achieved by SWaP with a wide variety of chemical systems tried, such as with various combinations of monomers, cross-linkers, photoinitiators, and nonreactive dye dopants. Next, we explored the ability to create more complex and arbitrary alignment patterns, such as four proof-of-concept common 2D target test patterns: a single radial alignment over a large area, an in-plane helical alignment, a low-symmetry alignment along the words "Tokyo Tech," and a microscopic and periodic radial alignment. These small-scale complex patterns of alignment with potential resolution down to the light diffraction limit, which could not be achieved over large areas by conventional photoalignment methods, demonstrate the great potential for SWaP for alignment pattern inscription in various applications, such as displays, soft actuators, energy harvesting, superresolution microscopy, coronagraphy, etc. Here, SWaP has been limited to photopolymerizable LCs, enabling large-area 1D and high-resolution 2D patterning, but in theory, SWaP is expected to act as a platform to align various materials as shown with light-absorbing (azobenzene) and light-emitting (oligothiophene) molecules. Furthermore, advantages in an industrial production setting are that this process is all-optical, single-step, noncontact, inexpensive, and, in general, applicable to incorporation directly into existing fabrication production lines.

RESULTS AND DISCUSSION

One-dimensional molecular alignment in LC polymer films by SWaP

As a typical example of SWaP for fabricating a 1D molecularly aligned LC polymer film, we 1D scanned a 250-μm-wide slit of ultraviolet (UV) light (λ = 365 nm; light intensity, 1.2 mW/cm^2; scanning rate, 20 μm/s) to initiate free-radical photopolymerization of a mixture (sample **1** including **M1**, **C1**, and **P1** in table S1, Fig. 2A, and figs. S1 to S3) in a handmade glass cell (2 cm × 2 cm) (refer also to Materials and Methods). The cell thickness was evaluated from its interference color (fig. S4) and was optimized for maximizing the degree of molecular alignment achieved by SWaP (fig. S5). The film was photopolymerized at 100°C, the temperature at which the resultant polymer shows an LC phase (fig. S6), and then cooled down to 25°C. The resultant film showed good optical transparency with no colored appearance (fig. S7). Polarized optical microscopy (POM) of the film under crossed polarizers displayed a clear contrast at every 45° rotation, and the image became completely dark when the polarization direction and the light scanning direction were parallel or perpendicular (Fig. 2B). Detailed POM observations with a tint plate with a retardation of 137 nm revealed that the film has uniform optical anisotropy with the slow axis along the light scanning direction, well within the range of typical birefringence levels required for current devices made of optical anisotropic, nematic LCs (*44*). This result implies that the emergence of birefringence with 1D slow axis was attributed to the 1D alignment of cyanobiphenyl moieties of the monomer **M1** along the light scanning direction. To more quantitatively investigate the details of the birefringence, we measured the polarized UV-visible (UV-vis) absorption spectra of the resultant film (Fig. 2C). Polar plots of the absorbance in the region of cyanobiphenyl moieties displayed the highest value along the scanning direction (Fig. 2D). We evaluated the in-plane orientation order parameter (*S*) from the equation $S = (A_{\parallel} - A_{\perp})/(A_{\parallel} + 2A_{\perp})$, where $A_{\parallel}$ and $A_{\perp}$ are defined as the absorbance in which the direction of polarized incident light was parallel or perpendicular to the light scanning direction, respectively. The *S* value found was 0.52, which is sufficient for fabrication, comparing well to levels achievable in similar chemical systems via conventional photoalignment methods (*13*, *28*–*30*). Further investigations using polarized infrared (IR) absorption spectra of the films, which were prepared to make them freestanding with a thickness of 4 μm, revealed that not only cyanobiphenyl moieties but also carbonyl moieties were aligned anisotropically throughout the film (Fig. 2E). Conversely, the alignment direction of carbonyl moieties was found to be perpendicular to that of the cyanobiphenyl moieties. This is reasonable and expected, because in common side-chain LC polymers, the side chains are aligned alongside their main chain under a shear-flow field (*45*–*47*) and, consequently, the carbonyl groups generally lie perpendicular to the polymer main chain (*30*, *48*). As a result, this suggests that SWaP causes alignment of the polymer main chains along the light scanning direction.

SWaP carried out above the isotropic clearing temperature of both monomers and resultant polymers was also able to induce 1D aligned

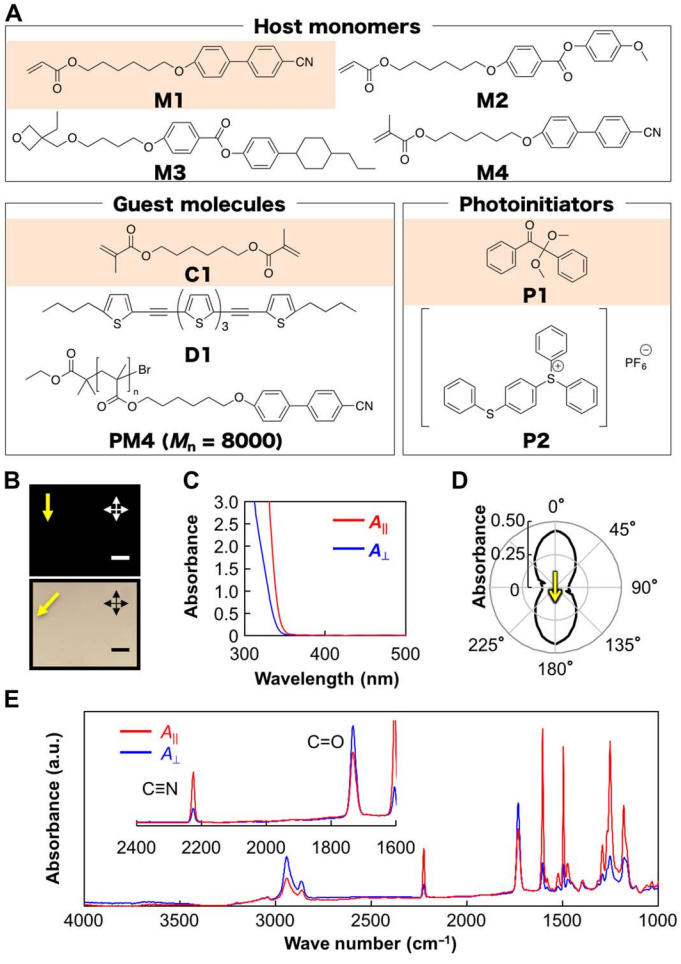

Fig. 2. Characterization of molecular alignment driven by SWaP of sample 1. (**A**) Chemical structures of materials used. The structures colored by orange rectangles are compounds for sample **1**. (**B**) POM images rotated by 45° from one another under crossed polarizers. Scale bars, 100 μm. Yellow arrows indicate the light scanning direction; black and white arrows depict the direction of the polarizers. (**C**) Polarized UV-vis absorption spectra, (**D**) a polar plot of UV-vis absorbance, and (**E**) polarized IR absorption spectra of a resultant film photopolymerized with light through a 250-μm slit scanned in 1D at 20 μm/s. For (C) and (D), the polar plot and order parameter are evaluated by averaging the UV-vis absorbance in a range of wavelength from 332 to 350 nm, measured by rotating the film every 5°. For (C) and (E), the azimuthal angle θ is defined as 0° for $A_{\parallel}$ and 90° for $A_{\perp}$ when the polarizing direction of incident light is parallel and perpendicular to the light scanning direction. a.u., arbitrary units.

LC polymer films by cooling down to room temperature (fig. S7). This behavior has not been previously observed in LCs using conventional photoalignment. Moreover, we notice that the polymer films showed a thermal memory effect of molecular alignment, recovering spontaneously after disappearing under heating above the isotropic clearing temperature (fig. S8). The results achieved by SWaP conducted under various thermal conditions and the thermal memory effect observed clearly support the idea that the polymer main chain aligns along the light scanning direction and might act as an anchor to align neighboring mesogens such as cyanobiphenyl moieties. Conversely, a film photopolymerized by spatiotemporally uniform light irradiation did not show uniform optical anisotropy but instead showed a polydomain structure that is typical for nematic LC polymers (fig. S9). These observations elucidate the power and importance of scanning light during photopolymerization for the 1D molecular alignment and the emergence of uniform optical anisotropy.

To confirm this alignment behavior, we directly observed the SWaP process via an in situ measurement by POM (fig. S10). Photopolymerization with a static slit light resulted in a microscopic molecular alignment only around the slit edge. On the other hand, during SWaP with a 1D scanned slit light, 1D optical anisotropy simultaneously emerged after photoirradiation, following the light scanning direction (movies S1 and S2). This result is plausible, assuming that molecular alignment is a result of a mass flow by molecular diffusion via a light gradient generating a distribution of resultant polymers, because scanning light enables the propagation of a reaction wavefront and a diffusion length, creating macroscopic molecular alignment. Moreover, we found that this process occurred successfully at scanning rates ranging between 2 and 68 μm/s, but the degree of molecular ordering decreased at lower and higher scanning rates (fig. S11). Lower scanning rates during photoirradiation might lead to a high polymer concentration to prevent molecular diffusion. On the other hand, higher scanning rates lead to lower polymer concentrations, which might reduce the diffusion rate and again decrease mass flow to induce molecular alignment. We achieved very fast processing at a high light intensity as discussed below.

Generality of SWaP in chemical systems

To demonstrate the generality of SWaP, molecular alignment was also achieved successfully in various other chemical systems attempted, as various combinations of monomers, cross-linkers, photoinitiators, and/or nonreactive dye dopants in a glass cell (samples **2** to **7** in table S1). We optimized the photopolymerization conditions regarding temperature, light intensity, and scanning rate to achieve the highest order parameter (figs. S1, S2, S6, and S11 to S13). POM observation of the resultant films revealed that all films photopolymerized with 1D scanned slit exhibited macroscopic uniform optical anisotropy where the slow axis was along the light scanning direction. Polarized UV-vis absorption spectra confirmed that the anisotropy again emerged from the 1D alignment of the anisotropic units (fig. S12). This means that SWaP has simplicity of processing and generality of materials design generation capabilities. The radical photopolymerization shown above can be commonly used because of its generality of materials design in monomers, cross-linkers, and initiators. However, oxygen needs to be inhibited in a glass cell or in a nitrogen atmosphere. To circumvent this issue, we used sample **5** including a cationic photoinitiator and a cationic photopolymerizable compound and conducted two SWaPs running under ambient conditions. We spin-coated a 40 weight % (wt %) propylene glycol monomethyl ether acetate (PGMEA) solution of sample **5** onto a glass substrate (size, 9 cm × 9 cm) and a flexible substrate (size, 2 cm × 3 cm) (refer also to Materials and Methods). We successfully produced 1D molecularly aligned polymer films by SWaP without a glass cell or a nitrogen atmosphere (fig. S13). Furthermore, the processing time for generating 1D alignment was much improved by using higher light intensity, and the scanning rate could be increased up to 900 μm/s at an intensity of 281 mW/cm^2, as shown in fig. S13B. Further improvement of the light scanning rate of 13.7 mm/s could be observed by using a higher light intensity of 458 mW/cm^2, as described in detail in the "Arbitrary 2D molecular alignment patterns by SWaP" section. The solution to further increase throughput rate could be an engineering optimization project for the future, but it does not represent a fundamental limitation at present.

Mechanism of molecular alignment by SWaP

The 1D molecular alignment achievable in these polymer films by SWaP can be rationalized by assuming that a light-triggered mass flow is the main driving force for the alignment, as schematically illustrated in Fig. 3A. Initially, monomers have only a random alignment. UV irradiation focused and guided on a selected region initiates photopolymerization and creates a spatial gradient of chemical potential, where macroscopic 1D diffusion of both monomers and polymers simultaneously takes place along the vector direction perpendicular to the boundary between polymerized and unpolymerized regions (*38*–*43*). Such a macroscopically directed diffusion induced under a nonequilibrium state causes 1D force, termed "thermodynamic force *F*," which enables one to induce macroscopic molecular flow along the diffusion direction (*49*–*51*). In SWaP, it is reasonable to assume that the 1D scanned light at a constant rate creates a stationary nonequilibrium state, in which a thermodynamic mass flow is maintained along the light scanning direction. This flow could impose shear stress on polymers to align their main chains along the flow direction (*45*–*47*), resulting in simultaneous alignment of neighboring anisotropic mesogens in the side chain. Finally, by UV irradiation throughout the film to complete photopolymerization and immobilize the resultant alignment, a stable macroscopic 1D molecularly aligned polymer film is obtained, in effect "frozen in." Conversely, the photopolymerization step with spatiotemporally uniform light, in polymer regions that were not scanned, immobilizes the initial random alignment of monomers, locking in their isotropy and resulting in a fixed polydomain structure.

This proposed mechanism is in good general agreement with the experimental observation that the light intensity and/or scanning rate in SWaP that is sufficient to reach a threshold of polymer concentration at the reaction wavefront is required to generate a diffusion-induced mass flow for the alignment of polymer main chains, which is a necessary step for the alignment of the LC units. However, other questions remain, such as what other factors caused by photopolymerization may also have an effect on molecular alignment. Other possible factors include evolved heat and volume shrinkage generating a mass flow (*52*, *53*).

To exclude the influence of these other possible factors, we designed a test photopolymerization system where two different mixtures were injected into a glass cell from each side toward its center by capillary force, so that we could generate a mass flow arising from diffusion at the boundary between them without any photopolymerization (Fig. 3B). As component mixtures, we used sample **6** including **M4** and **P1** and, in addition to **6**, sample **7** including the polymer of **PM4** [M_n (number-average molecular weight) = 8000] synthesized by atom transfer radical polymerization (ATRP) of **M4** (fig. S14 and table S2) (refer also to Materials and Methods). After various durations of 0, 30, 60, and 180 s from contact, we conducted the photopolymerization steps with spatiotemporally uniform light throughout the glass cell to immobilize any molecular alignment induced by diffusion at the boundary. POM observation of these test films revealed that 1D molecular alignment was induced at and perpendicular to the boundary where the alignment direction was coincident with the diffusion direction. Increasing the contacting duration increased both the alignment length and the level of birefringence until these two values reached 800 μm and 0.08, respectively (Fig. 3, C and D, and fig. S15). The birefringence obtained is similar to that generated by SWaP. In the test cases, photopolymerization occurs uniformly because of the photoirradiation throughout the glass cell. Evolved heat and the volume shrinkage are expected to be uniform in the glass cell. As a result, the effect of these factors on both mass flow

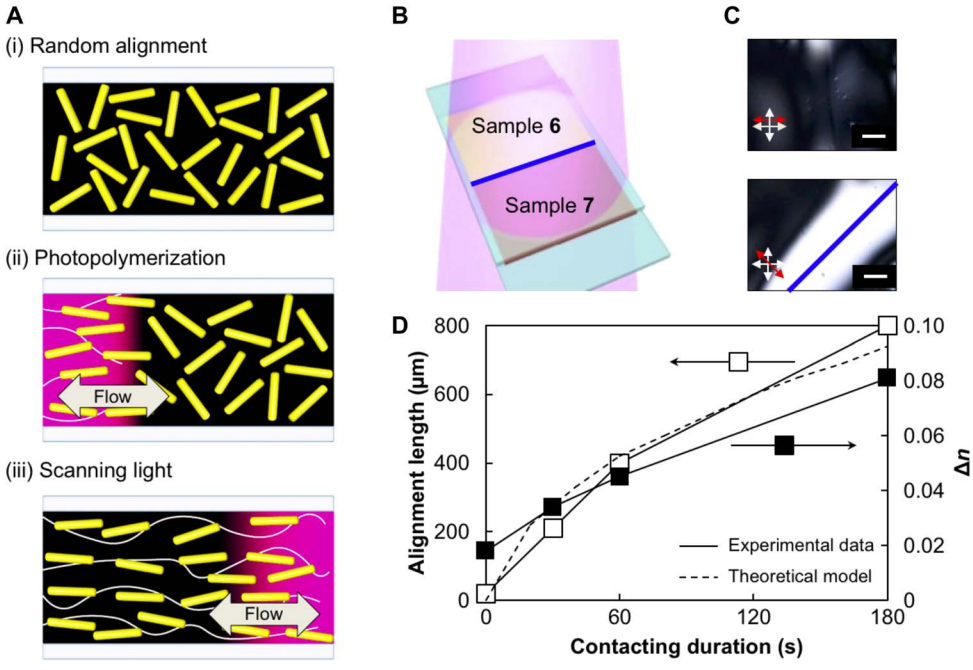

Fig. 3. Evidence that molecular diffusion drives alignment. (**A**) Schematic illustrations of the generation of molecular alignment during SWaP where a mass flow triggered by photopolymerization aligns both the mesogenic side-chain units (yellow rod) and the polymer main chains (white curves) over large areas depending on scanning light. (**B**) A schematic illustration of photopolymerization at the boundary (blue line) of two mixtures injected into a glass cell from separate sides. (**C**) POM images under crossed polarizers offset 0° (top) and −45° (bottom) from vertical of resultant films photopolymerized 180 s after contacting the two mixtures. Red arrows show the injection direction; white arrows show the direction of polarizers. Scale bar, 200 μm. (**D**) Alignment length and birefringence emerged as a function of flow duration compared with a theoretical model.

and molecular alignment could be negligible. This clearly suggests that the concentration difference of polymers is the main driving force and has the ability to align molecules strongly, perpendicular to the boundary.

To further quantify the proposed mechanism, we also compared the observed data with a theoretical model of alignment length resulting from molecular diffusion based on Fick's law of diffusion (Fig. 3D and fig. S16) (*49*). In all materials, when there is a difference of chemical potential, for example, arising from a difference of molecular concentrations, the molecules diffuse to reach an equilibrium state. The change of the concentration due to diffusion is described by the following equation

$$\frac{\partial c}{\partial t} = D\frac{\partial^2 c}{\partial x^2} \tag{1}$$

where c denotes the molecular concentration (mol m^{-3}), t denotes the duration time (s), D denotes a diffusion coefficient (m^2 s^{-1}), and x denotes the diffusion length (m). Under our experimental conditions, molecules diffuse in 1D, and Eq. 1 can be readily transformed into a predictive form for concentration

$$c(x,t) = \frac{n_0}{A(\pi Dt)^{1/2}} e^{-x^2/4Dt} \tag{2}$$

where A denotes the area of the boundary of two mixtures (m^2), n_0 estimates the total amounts of molecules (= N_0/N_A, where N_A is Avogadro's number), and the following equation describes a diffusion coefficient D, estimated by the Stokes-Einstein relation

$$D = \frac{kT}{6\pi\eta a} \tag{3}$$

where k represents the Boltzmann constant (kg m^2 K^{-1} s^{-2}), T represents the temperature (K), η represents the viscosity of the solvent (kg m^{-1} s^{-1}), and a represents the molecular radius of the solute (m). Values for all these parameters were selected on the basis of current experimental determination or from previous literature (*54*–*56*). To estimate the molecular alignment length arising from molecular diffusion, we assumed the theoretical alignment length as the sum of diffusion lengths of monomers and polymers. The experimental data suggest that the molecular alignment starts when a certain amount of polymer causes sufficient diffusion and mass flow to impose shear stress on the polymers. Therefore, we calculated the existence probability dP of monomers and polymers in a volume element ($dV = Adx$, where dx is the length element along the diffusion direction) by using Eqs. 2 and 3 (refer also to Supplementary Materials).

$$dP = \frac{c}{n_o} dV = \frac{(\pi Dt)^{1/2}}{e^{-x^2/4Dt}} dx \tag{4}$$

Here, we defined the theoretical alignment length as the diffusion length when the integration of P became 85%. As shown in Fig. 3D and fig. S16, this theoretical analysis agrees very well with the experimental data. The correlation of molecular alignment length by the test system and the theoretical model appears quantitatively to support the mechanism of molecular alignment by diffusion.

Although there exists a difference between the test system using low-weight polymers and the real situation of SWaP producing cross-linked LC polymers, we have experimentally proved that the molecular alignment length scale reached a comparable level of hundreds of micrometers. We observed in situ the photopolymerization process of sample **1** under crossed polarizers. This experiment revealed that the film photopolymerized with a static slit light had molecular alignment, which was induced not only in the irradiated region but also spread out even to unirradiated regions. The alignment length became much longer as the photopolymerization duration was increased, and the length scale reached hundreds of micrometers. By observation of the surface profile of the polymer film obtained, we found that the surface became embossed, and the apex of the embossed surface was located in the center of the irradiated regions. These experimental results mean that both the monomers and the resultant polymers showed a directed mass transport between the polymerized and the nonpolymerized regions and could generate molecular alignment around the boundary.

Arbitrary 2D molecular alignment patterns by SWaP

Last, we explored the generation of arbitrary 2D alignment patterns by introducing further complexity in spatiotemporal scanning of incident light during SWaP, where light-triggered diffusion governs alignment. We defined SWaP as photopolymerization with spatially or temporally scanned light to generate the molecular alignment by molecular diffusion in the nonequilibrium state. This means that even patterned irradiation, such as a grating, a lattice, a honeycomb, etc., could enable various complex molecular alignment patterning as a result of diffusion at the edge of the mask.

To precisely design macroscopic or further complex 2D patterns of molecular alignment, we used a digital micromirror device (DMD) as a spatiotemporally arbitrary photomask for SWaP of sample **1** in a glass cell (refer also to Materials and Methods). As representatives, we first aimed to inscribe three test alignment patterns over large areas as shown in Fig. 4A: (I) a macroscopic radial alignment, (II) an in-plane helical alignment where the helical axis was perpendicular to the light scanning direction, and (III) low-symmetry alignment along the words "Tokyo Tech." Figure 4B shows the schematic illustrations of how we spatiotemporally scanned incident light: (I) 2D "toroid-shaped" scanning, (II) 1D scanning of periodic dots, and (III) a 2D scan along the words (fig. S17 and movies S3 to S5). As was previously mentioned, to generate a uniform molecular alignment, SWaP requires precise control of the light intensity and the light scanning rate during the process, and thus, we optimized the parameters from criteria of the resultant retardation in films. POM observation of the resultant films under optimized conditions revealed that they had the 2D complex alignment patterns over large areas as expected (Fig. 4, C and D). All films had complex molecular alignment when the light was scanned; we observed unidirectional molecular alignment along the light scanning direction within the irradiated regions, but at the edge of the irradiated regions, molecular alignment direction became perpendicular to the scanning direction. We obtained a symmetric uniform radial pattern by 2D expansion of a circle as shown in pattern I. In patterns II and III, we designed more complex patterns with low symmetry due to the spatial integration of the helical molecular alignment.

In addition to large-area alignment patterns, we further demonstrated the design of microscopic alignment patterns by SWaP. We used an optical image (pattern IV), which is a square lattice with a lattice point distance of 27.4 μm and an irradiated region width of 13.7 μm, as shown in Fig. 5A. POM observations of the resultant film revealed

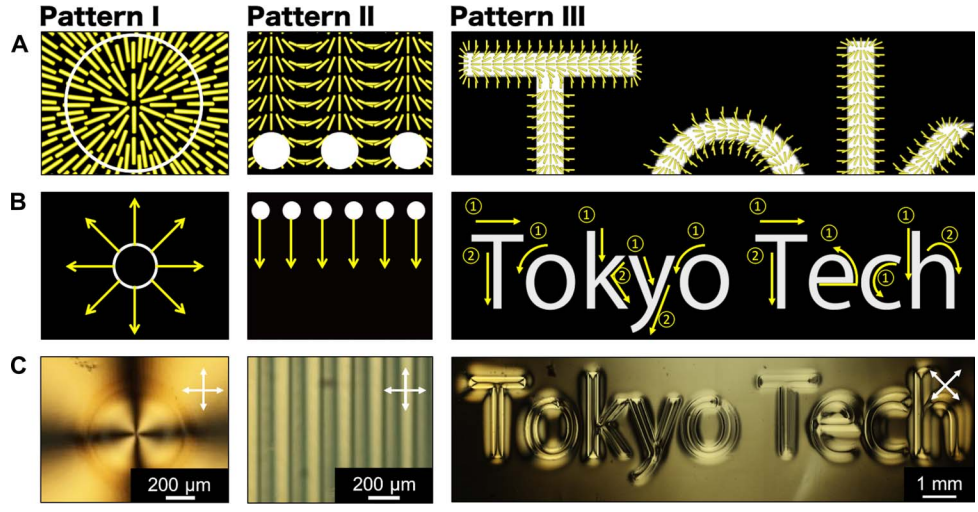

Fig. 4. Arbitrary alignment patterns developed by spatiotemporal scanning of light. (**A**) Schematic illustrations of desired patterns of alignment of mesogenic side-chain unit (yellow rod). (**B**) Irradiated light patterns: (I) toroid shape expanding at 27.4 μm/s with a width of 247 μm and a diameter of 493 μm in the initial state; (II) periodic dots scanned in 1D at 27.4 μm/s with a diameter of 137 μm and a center-to-center distance of 206 μm; and (III) the words "Tokyo Tech" where 178-μm-wide light was scanned at 13.7 mm/s and an exposure time of 1 min. White and black areas represent irradiated and unirradiated regions. The yellow arrows show the scanning direction, and the numbers denote the scanning order. (**C**) POM images under crossed polarizers. White arrows show the direction of polarizers.

that the film had an array pattern of radial alignment. The size of each radial alignment was ~27.4 μm, maintaining the same periodicity as a square lattice of irradiated pattern. Of particular interest is that the size of each radial alignment obtained in the film of pattern IV is much smaller (by a factor of 10^4) than that obtained via conventional photoalignment methods. Furthermore, the number of radial alignment patterns reached 500 × 300 throughout the film. In comparison, conventional methods use a laser beam to control a pixel with a size of 0.01 mm^2, and consequently, the smallest size of each radial alignment pattern rises up to square millimeters (*2*, *33*, *57*).

Furthermore, to explore the highest resolution achievable by SWaP, we used a commercially available test-target photomask, as shown in Fig. 5B. We prepared a cell fabricated by adhering a glass substrate and a test target with glue including a 2-μm-thick spacer. Then, we conducted SWaP of sample **1** in the cell with UV light irradiated from the test-target side at an intensity of 100 mW/cm^2 and an exposure time of 3 min. After SWaP, the polymer film was obtained by opening the cell. POM observation of the resultant film revealed that the film had a molecular alignment pattern in the same manner as the test-target pattern used (Fig. 5B). In the masked region, the film exhibited a radial molecular alignment pattern. It is noteworthy that even in the smallest masked region of the test-target pattern with a 2-μm line-space pattern, the resultant polymer film showed the radial alignment patterns, indicating that molecular alignment by SWaP enables high-resolution patterning.

These resultant alignment patterns (I to IV) have potential application in more complex photonic and mechanical devices. For example, in photonic applications, patterns I and IV could be a vortex retarder converting a polarized beam into a vector vortex beam, which is essential in stimulated emission depletion microscopy and nanomanipulation, and pattern IV has great potential to reduce processing time for these technologies. Furthermore, pattern II represents potential materials for next-generation displays because of a specific light scattering phenomenon where a coherent linearly polarized beam can be completely scattered as left and right circularly polarized beams into +first and −first order, respectively (*58*, *59*). Last, for photomechanical applications, these patterns might be used as stimuli-responsive soft-actuator components important for microfluidics and solar energy harvesting and conversion because these molecularly aligned films permit a repeatable shape change depending on their alignment patterns (*2*, *14*–*16*).

These complex alignment patterns achieved over large areas not only allow easy processing of these 2D patterns but also have industrial advantages that include all-optical, single-step, noncontact, inexpensive, and general applicability to existing materials in existing fabrication production lines without extra steps such as surface treatment, electrodes, or polarized light sources.

CONCLUSION

We have demonstrated that single-step processing of arbitrary 2D alignment patterns over large areas is readily achieved by SWaP without any surface treatment, electrodes, or polarized light sources and offers great potential for the fabrication of a variety of high-performance LC devices. Of particular interest here is the opportunity to inscribe complex 2D patterns with high resolution down to ~2 μm, because this is challenging or even impossible to achieve with conventional photoalignment techniques, requiring instead the use of complicated and expensive holographic technologies or a dynamic control of polarized light. However, the SWaP described here is triggered only by a simple mass flow arising from molecular diffusion, evident from experimental and theoretical results, and could work easily and economically as a chemical system platform for controlling the alignment of a wide variety of LCs. Although SWaP is currently limited to photopolymerizable LC systems with thicknesses below tens of micrometers, further investigations will expand material systems used either by a two-step method where the resultant polymer film could be used as a template to align LCs even with thicknesses above hundreds of micrometers coated over the template or by enhancing a mass flow to align other anisotropic materials, such as nanorods, nanocarbons, and proteins. Furthermore, SWaP also has great economic advantages that can be readily introduced in existing photoproduction facilities. We believe that SWaP provides a new, general, and powerful pathway for the simple creation of highly functional

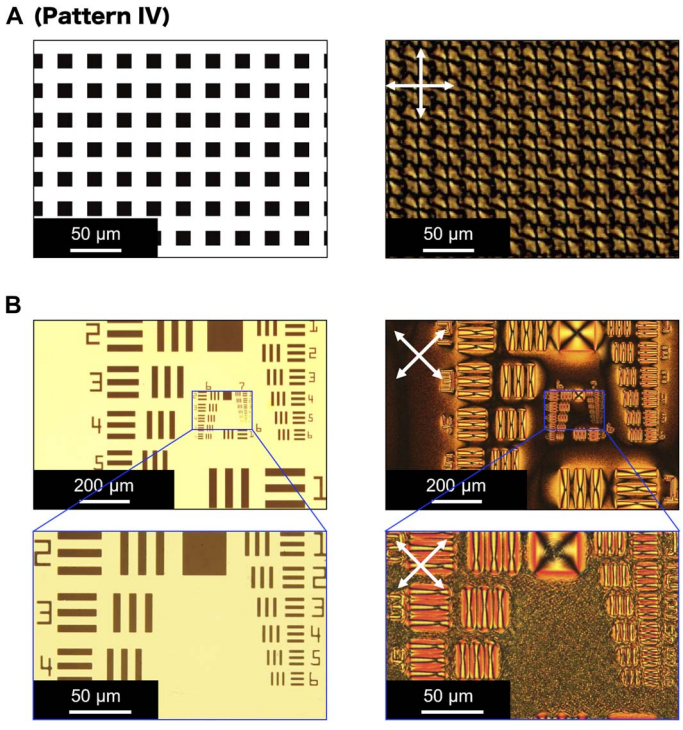

Fig. 5. High-resolution patterning of molecular alignment by SWaP. (**A**) An optical pattern of a square lattice with a lattice point distance of 27.4 μm and an irradiated region width of 13.7 μm (left), and POM images of the resultant polymer film displaying an array of microscopic radial molecular alignment (right). (**B**) Photograph of a test target used as a photomask having the highest resolution of ~2-μm line space (left), and a POM image of the resultant polymer film (right). For (B), the bottom images are higher magnifications of the top images. White arrows show the direction of polarizers.

organic materials with arbitrary, fine molecular alignment patterns in nanoscale over large areas.

MATERIALS AND METHODS

Chemical materials

Unless otherwise stated, all reagents and solvents were purchased from commercial suppliers and used as received, including tetrahydrofuran (THF), dimethylformamide, ethyl acetate, chloroform, hexane, 2-propanol, PGMEA, radical photoinitiator Irgacure 651 (**P1**), and cationic photoinitiator CPI-100 (**P2**). The monomers 4′-[6-(acryloyloxy)hexyloxy]-4-cyanobiphenyl (**M1**), 4′-methoxyphenyl 4-[6-(acryloyloxy)hexyloxy] benzoate (**M2**), and 4-(4-propylcyclohexyl)phenyl 4-(4-((3-ethyloxetan-3-yl)methoxy)butoxy)benzoate (**M3**) were washed through the following steps. First, they were dissolved in a sufficient amount of chloroform, and then the solution was stirred at 25°C for 1 hour. The solutions were then purified using column chromatography (SiO_2 and chloroform) where the first fraction was collected and evaporated to dryness, and the resultant solid was recrystallized from THF/hexane and finally dried at 25°C for 24 hours under reduced pressure to provide monomers **M1**, **M2**, and **M3** as white solids. 1,6-Bis(methacryloyloxy)hexane (**C1**) was washed with a 5 wt % sodium hydroxide solution in water. The solution was dried over anhydrous magnesium sulfate and purified using filtration, and the product was obtained. 4′-[6-(Methacryloyloxy) hexyloxy]-4-cyanobiphenyl (**M4**) was synthesized as described in texts S1 and S2, and 5,5″-bis-(5-butyl-2-thienylethynyl)-2,2′:5′,2″-terthiophene (**D1**) was synthesized according to previously reported methods (*60*).

General characterization methods

Nuclear magnetic resonance (NMR) spectroscopy was performed on a spectrometer (Bruker, AVANCE III 400A; 400.0 MHz for ^1H) in 16 steps using tetramethylsilane as the internal reference for deuterated chloroform solutions. Differential scanning calorimetry (DSC) was performed with a DSC200C (SEIKO Instruments). DSC scans were performed within certain temperature ranges at a heating rate of 1.0 or 10°C/min under nitrogen for monomer mixtures or polymers, respectively. Approximately 5.0 and 10.0 mg were used for DSC measurements for all samples and for resultant polymers, respectively. An empty aluminum pan was used as a reference. The phase transition temperature behavior of all samples and resultant polymers is summarized in fig. S6 and table S1. Optical anisotropic properties such as birefringence (Δn) and the optical axis of molecularly aligned polymer films were evaluated with a polarized optical microscope (Olympus, BX50) equipped with a hot stage (Mettler, FP-90 and FP-82HT) and a Berek compensator (Olympus, U-CBE) or a tint plate (Olympus, U-TP137) (*61*). Absorption, transmittance, and polarized absorption spectra of resulting polymer films were measured using a UV-vis spectrophotometer (JASCO, V-650ST) and an IR spectrophotometer (JASCO, FT/IR-6100) equipped with a rotatable film holder and a polarizer. Using the UV-vis measurements, we quantitatively evaluated the degree of molecular alignment described in the "Evaluation of the degree of molecular alignment" section.

ATRP of M4

A well-defined polymer (**PM4**) was synthesized by ATRP (*62*) of the monomer (**M4**) in a dry anisole solution under an argon atmosphere using ethyl 2-bromoisobutyrate (EBrIB) as an initiator and CuCl/1,1,4,7,10,10-hexamethyltriethylenetetramine as a ligand. The reaction medium was heated at 90°C for 24 hours and cooled down to 25°C. The sample composition and detailed characterization of the resultant polymers are summarized in table S2. The resulting polymer was purified by reprecipitation. The white solid product was dried under reduced pressure. The M_n and M_w (weight-average molecular weight) and the conversion were determined by gel permeation chromatography (GPC; JASCO, DG-2080-53; column: Shodex, GPC LF804 + LF804 + LF804A; solvent: chloroform) (fig. S14). Unless otherwise noted, we used the polymer with M_n = 8000 (conversion: 72%) for the work presented in this paper.

Sample preparation

Sample mixtures were composed of a host monomer, a guest, and a photoinitiator, at a desired ratio. The three components were dissolved in THF and were stirred at 25°C for 30 min. The solutions were dried under reduced pressure and resulted in recovery of solid products. The compositions of all samples, except for sample **5** because it was mixed in weight ratio, were determined by ^1H NMR, with results summarized in table S1. In all cases, a small amount of the mixture solution was measured, and the component ratio was calculated using the integral of signals corresponding to components, relative to the amount of monomer (fig. S3).

Fabrication of glass cells

Glass substrates were cleaned through the following steps. First, 25-mm × 25-mm glass substrates were cleaned ultrasonically in three consecutive steps with 1.0 wt % neutral detergent (KANTO KAGAKU, Cica Clean

LX-II) in water, with distilled water, and with 2-propanol. Subsequently, the cleaned substrates were dried under ambient conditions for 24 hours. Second, the substrates were treated by UV-ozone cleaner (TAKEDA, NL-UV42) for 10 min. Next, glass cells were fabricated manually by adhering two substrates with glue separated by 2- to 5-μm-thick silica spacers (Thermo Scientific, 9000 Series). The thickness of a cell was determined by UV-vis spectroscopy on the basis of the Fabry-Perot measurement method (*63*). A representative result and the equation used for the calculation are shown in fig. S4.

SWaP with a 4f optical setup in a glass cell or on a substrate

Photopolymerization processes can be classified into two groups according to the type of surrounding conditions: those conducted with samples in the handmade glass cells and those on a substrate under ambient conditions. Solid-state samples were prepared by melting the material above its isotropic temperature on a hot stage and then injecting the hot liquid by capillary force into a glass cell. Substrate samples were prepared by spin-coating a 40 wt % solution in PGMEA, including the leveling agent (DIC, MEGAFAC R-40) at 1000 parts per million at 25°C at a spinning rate of 400 rotations per minute (rpm) for 5 s followed by ramping up to 800 rpm for 30 s, and were then dried above its isotropic temperature for 2 min. The samples were then cooled down to the photopolymerization temperature. Unless otherwise noted, the photopolymerization temperature was chosen to be in the range of the LC temperature of the resultant polymer (figs. S6 and S7), and the film thickness was 2 to 3 μm, which was optimized, as shown in fig. S5. Unless otherwise stated, the sample was irradiated with 365-nm UV light (USHIO, USH-500SC) normal to the surface, through glass filters (AGC Techno Glass, IRA-25S, UV-36A) and neutral density filters (fig. S1A). During SWaP, unless otherwise stated, the cell was irradiated with UV light through a slit mask (width, 250 μm), 1D scanned at 20 μm/s, and subsequently irradiated throughout to complete polymerization and fix the resultant molecular alignment, under optimized exposure conditions, as shown in figs. S11 to S13. Finally, the resultant polymer film was annealed for 2 min above its isotropic temperature and rapidly cooled down below its glass transition temperature in liquid nitrogen.

SWaP using a DMD

Photopolymerization of sample **1** in a glass cell was conducted with a UV-LED (light-emitting diode) equipped with a DMD (ViALUX, DLP Projection module HP-LED-OM-XS-UV-λ), as the UV light source and a dynamic mask, instead of the combination of a UV lamp and a commercially available photomask used as described in the "SWaP with a 4f optical setup in a glass cell or on a substrate" section. A DMD enables one to easily generate arbitrary spatiotemporal light patterns (*64*). The cell was irradiated using 390-nm UV-LED light (fig. S1B), having a pattern designed by Illustrator software (Figs. 4 and 5, fig. S17, and movie S2). The light intensity depended on the irradiated pattern: for pattern I, 10 mW/cm^2; for pattern II, 60 mW/cm^2; for pattern III, 458 mW/cm^2; and for pattern IV, 10 mW/cm^2. Other photopolymerization conditions and procedures were the same as described previously.

Evaluation of the degree of molecular alignment

The degree of in-plane alignment of oriented molecules, referred to as the order parameter (S), was estimated from the polarized UV-vis absorption spectra by the following equation (*44*): $S = (A_{||} - A_{\perp})/(A_{||} + 2A_{\perp})$. Here, $A_{||}$ and $A_{\perp}$ are the absorption values obtained through measurements using incident polarized light that was either parallel or perpendicular to the light scanning direction, respectively.

SUPPLEMENTARY MATERIALS

Supplementary material for this article is available at http://advances.sciencemag.org/cgi/content/full/3/11/e1701610/DC1

text S1. Synthesis of 4′-hydroxyhexyl-4-cyanobiphenyl (compound **1**)
text S2. Synthesis of 4′-[6-(methacryloyloxy)hexyloxy]-4-cyanobiphenyl (**M4**)
text S3. Theoretical estimation of molecular alignment length
fig. S1. Schematic illustrations of the optical setup for SWaP.
fig. S2. UV-vis absorption spectra of monomers, guest molecules, and photoinitiators in THF.
fig. S3. Representative ^{1}H NMR spectrum of a sample of **1**.
fig. S4. A plot of transmittance as a function of wavelength to determine the thickness of a handmade glass cell.
fig. S5. The effect of cell thickness on molecular alignment behavior in SWaP of sample **1**.
fig. S6. DSC thermograms of monomers and homopolymers.
fig. S7. Effect of photopolymerization temperature on molecular alignment behavior in SWaP of sample **1**.
fig. S8. Thermal memory effect on molecular alignment generated by SWaP of sample **1**.
fig. S9. Photopolymerization of sample **1** without spatiotemporal scanning of light.
fig. S10. Schematic illustration of the optical setup for in situ observation during SWaP.
fig. S11. Effect of the light scanning rate on the order parameter (S) in SWaP of sample **1**.
fig. S12. Demonstration of the generality of SWaP for various chemical systems with the 4f optical setup with a high-pressure mercury lamp.
fig. S13. Demonstration of the robustness of SWaP using cationic polymerization.
fig. S14. GPC chromatogram for **PM4** (M_n = 8000) detected at 300 nm.
fig. S15. Emergence of molecular alignment without SWaP in the test case.
fig. S16. Theoretical model of alignment length and molecular diffusion length in the test case estimated from Fick's law of diffusion.
fig. S17. Two dimensional and 3D intensity profiles of the representative patterns irradiated with a DMD captured with a charge-coupled device beam profiler.
table S1. Composition ratios of materials and thermodynamic properties of the samples used in this study.
table S2. Molecular weights of polymers prepared by ATRP.
movie S1. In situ observation of SWaP with 1D scanned slit light of sample **1**.
movie S2. In situ observation of static photopolymerization with slit light of sample **1**.
movie S3. An irradiated pattern designed by Illustrator software for SWaP with a 2D expanding "toroid-shape."
movie S4. An irradiated pattern designed by Illustrator software for SWaP with a 1D scanning of periodic dots.
movie S5. An irradiated pattern designed by Illustrator software for SWaP with 2D scanning along various letters.

REFERENCES AND NOTES

1. R. Lakes, Materials with structural hierarchy. *Nature* **361**, 511–515 (1993).
2. T. J. White, D. J. Broer, Programmable and adaptive mechanics with liquid crystal polymer networks and elastomers. *Nat. Mater.* **14**, 1087–1098 (2015).
3. A. R. Hirst, B. Escuder, J. F. Miravet, D. K. Smith, High-tech applications of self-assembling supra-molecular nanostructured gel-phase materials: From regenerative medicine to electronics devices. *Angew. Chem. Int. Ed.* **47**, 8002–8018 (2008).
4. S. J. Woltman, G. D. Jay, G. P. Crawford, Liquid-crystal materials find a new order in biomedical applications. *Nat. Mater.* **6**, 929–938 (2007).
5. M. O'Neill, S. M. Kelly, Liquid crystals for charge transport, luminescence, and photonics. *Adv. Mater.* **15**, 1135–1146 (2003).
6. J.-M. Lehn, Toward self-organization and complex matter. *Science* **295**, 2400–2403 (2002).
7. T. Kato, Self-assembly of phase-segregated liquid crystal structures. *Science* **295**, 2414–2418 (2002).
8. G. M. Whitesides, B. Grzybowski, Self-assembly at all scales. *Science* **295**, 2418–2421 (2002).
9. T. Kato, N. Mizoshita, K. Kishimoto, Functional liquid-crystalline assemblies: Self-organized soft materials. *Angew. Chem. Int. Ed.* **45**, 38–68 (2006).
10. M. Schadt, Milestone in the history of field-effect liquid crystal displays and materials. *Jpn. J. Appl. Phys.* **48**, 03B001 (2009).
11. O. Yaroshchuk, Y. Reznikov, Photoalignment of liquid crystals: Basics and current trends. *J. Mater. Chem.* **22**, 286–300 (2012).
12. T. Seki, S. Nagano, M. Hara, Versatility of photoalignment techniques: From nematics to a wide range of functional materials. *Polymer* **54**, 6053–6072 (2013).
13. V. G. Chigrinov, V. M. Kozenkov, H.-S. Kwok, *Photoalignment of Liquid Crystalline Materials: Physics and Applications* (Wiley, 2008).
14. A. Priimagi, C. J. Barrett, A. Shishido, Recent twists in photoactuation and photoalignment control. *J. Mater. Chem. C* **2**, 7155–7162 (2014).
15. T. Seki, Light-directed alignment, surface morphing and related processes: Recent trends. *J. Mater. Chem. C* **4**, 7895–7910 (2016).

16. J.-A. Lv, Y. Liu, J. Wei, E. Chen, L. Qin, Y. Yu, Photocontrol of fluid slugs in liquid crystal polymer microactuators. *Nature* **537**, 179–184 (2016).
17. J. Kobashi, H. Yoshida, M. Ozaki, Planar optics with patterned chiral liquid crystals. *Nat. Photon.* **10**, 389–392 (2016).
18. S. Palagi, A. G. Mark, S. Y. Reigh, K. Melde, T. Qiu, H. Zeng, C. Parmeggiani, D. Martella, A. Sanchez-Castillo, N. Kapernaum, F. Giesselmann, D. S. Wiersma, E. Lauga, P. Fischer, Structured light enables biomimetic swimming and versatile locomotion of photoresponsive soft microrobots. *Nat. Mater.* **15**, 647–653 (2016).
19. A. H. Gelebart, D. J. Mulder, M. Varga, A. Konya, G. Vantomme, E. W. Meijer, R. L. B. Selinger, D. J. Broer, Making waves in a photoactive polymer film. *Nature* **546**, 632–636 (2017).
20. T. Todorov, L. Nikolova, N. Tomova, Polarization holography. 1: A new high-efficiency organic material with reversible photoinduced birefringence. *Appl. Opt.* **23**, 4309–4312 (1984).
21. K. Ichimura, Y. Suzuki, T. Seki, A. Hosoki, K. Aoki, Reversible change in alignment mode of nematic liquid crystals regulated photochemically by command surfaces modified with an azobenzene monolayer. *Langmuir* **4**, 1214–1216 (1988).
22. W. M. Gibbons, P. J. Shannon, S.-T. Sun, B. J. Swetlin, Surface-mediated alignment of nematic liquid crystals with polarized laser light. *Nature* **351**, 49–50 (1991).
23. M. Schadt, K. Schmitt, V. Kozinkov, V. Chigrinov, Surface-induced parallel alignment of liquid crystals by linearly polymerized photopolymers. *Jpn. J. Appl. Phys.* **31**, 2155–2164 (1992).
24. M. Schadt, H. Seiberle, A. Schuster, S. M. Kelly, Photo-induced alignment and patterning of hybrid liquid crystalline polymer films on single substrates. *Jpn. J. Appl. Phys.* **34**, L764–L767 (1995).
25. A. V. Medvedev, E. B. Barmatov, A. S. Medvedev, V. P. Shibaev, S. A. Ivanov, M. Kozlovsky, J. Stumpe, Phase behavior and photooptical properties of liquid crystalline functionalized copolymers with low-molecular-mass dopants stabilized by hydrogen bonds. *Macromolecules* **38**, 2223–2229 (2005).
26. M. Nishikawa, B. Taheri, J. L. West, Mechanism of unidirectional liquid-crystal alignment on polyimides with linearly polarized ultraviolet light exposure. *Appl. Phys. Lett.* **72**, 2403–2405 (1998).
27. K. Kumagai, K. Sakamoto, K. Usami, R. Arafune, Y. Nakabayashi, S. Ushioda, Molecular orientation of liquid crystal monolayers on polyimide films exposed to linearly polarized UV light. *Jpn. J. Appl. Phys.* **38**, 3615–3618 (1999).
28. N. Kawatsuki, T. Washio, J. Kozuki, M. Kondo, T. Sasaki, H. Ono, Photoinduced orientation of photoresponsive copolymers with *N*-benzylideneaniline and nonphotoreactive mesogenic side groups. *Polymer* **56**, 318–326 (2015).
29. T. Seki, New strategies and implications for the photoalignment of liquid crystalline polymers. *Polym. J.* **46**, 751–768 (2014).
30. Y. Wu, Y. Demachi, O. Tsutsumi, A. Kanazawa, T. Shiono, T. Ikeda, Photoinduced alignment of polymer liquid crystals containing azobenzene moieties in the side chain. 2. Effect of spacer length of the azobenzene unit on alignment behavior. *Macromolecules* **31**, 1104–1108 (1998).
31. M. Schadt, H. Seiberle, A. Schuster, Optical patterning of multi-domain liquid-crystal displays with wide viewing angles. *Nature* **381**, 212–215 (1996).
32. K. Fukuhara, S. Nagano, M. Hara, T. Seki, Free-surface molecular command systems for photoalignment of liquid crystalline materials. *Nat. Commun.* **5**, 3320 (2014).
33. T. H. Ware, M. E. McConney, J. J. Wie, V. P. Tondiglia, T. J. White, Voxelated liquid crystal elastomers. *Science* **347**, 982–984 (2015).
34. V. K. Gupta, N. L. Abbott, Design of surfaces for patterned alignment of liquid crystals on planar and curved substrates. *Science* **276**, 1533–1536 (1997).
35. Y. Xia, G. Cedillo-Servin, R. D. Kamien, S. Yang, Guided folding of nematic liquid crystal elastomer sheets into 3D via patterned 1D microchannels. *Adv. Mater.* **28**, 9637–9643 (2016).
36. R. Lin, J. A. Rogers, Molecular-scale soft imprint lithography for alignment layers in liquid crystal devices. *Nano Lett.* **7**, 1613–1621 (2007).
37. M. Reznikov, A. Sharma, T. Hegmann, Ink-jet printed nanoparticle alignment layers: Easy design and fabrication of patterned alignment layers for nematic liquid crystals. *Part. Part. Syst. Charact.* **31**, 257–265 (2014).
38. K. Hisano, Y. Kurata, M. Aizawa, M. Ishizu, T. Sasaki, A. Shishido, Alignment layer-free molecular ordering induced by masked photopolymerization with non-polarized light. *Appl. Phys. Express* **9**, 072601 (2016).
39. V. V. Krongauz, E. R. Schmelzer, R. M. Yohannan, Kinetics of anisotropic photopolymerization in polymer matrix. *Polymer* **32**, 1654–1662 (1991).
40. D. J. Broer, J. Lub, G. N. Mol, Wide-band reflective polarizers from cholesteric polymer networks with a pitch gradient. *Nature* **378**, 467–469 (1995).
41. R. A. M. Hikmet, H. Kemperman, Electrically switchable mirrors and optical components made from liquid-crystal gels. *Nature* **392**, 476–479 (1998).
42. R. L. Sutherland, V. P. Tondiglia, L. V. Natarajan, T. J. Bunning, Phenomenological model of anisotropic volume hologram formation in liquid-crystal-photopolymer mixtures. *J. Appl. Phys.* **96**, 951–965 (2004).
43. C. M. Leewis, A. M. de Jong, L. J. van IJzendoorn, D. J. Broer, Reaction–diffusion model for the preparation of polymer gratings by patterned ultraviolet illumination. *J. Appl. Phys.* **95**, 4125–4139 (2004).
44. D. Demus, J. W. Goodby, G. W. Gray, H.-W. Spiess, V. Vill, *Handbook of Liquid Crystals* (Wiley-VCH, 1998).
45. S. V. Fridrikh, E. M. Terentjev, Polydomain-monodomain transition in nematic elastomers. *Phys. Rev. E* **60**, 1847–1857 (1999).
46. C. Pujolle-Robic, L. Noirez, Observation of shear-induced nematic-isotropic transition in side-chain liquid crystal polymers. *Nature* **409**, 167–171 (2001).
47. A. Agrawal, A. C. Chipara, Y. Shamoo, P. K. Patra, B. J. Carey, P. M. Ajayan, W. G. Chapman, R. Verduzco, Dynamic self-stiffening in liquid crystal elastomers. *Nat. Commun.* **4**, 1739 (2013).
48. B. R. Nair, V. G. Gregoriou, P. T. Hammond, FT-IR studies of side chain liquid crystalline thermoplastic elastomers. *Polymer* **41**, 2961–2970 (2000).
49. P. Atkins, J. de Paula, *Atkins' Physical Chemistry* (Oxford Univ. Press, ed. 8, 2006).
50. R. D. Astumian, Thermodynamics and kinetics of a Brownian motor. *Science* **276**, 917–922 (1997).
51. A. Würger, Thermal non-equilibrium transport in colloids. *Rep. Prog. Phys.* **73**, 126601 (2010).
52. J. P. Singer, P.-T. Lin, S. E. Kooi, L. C. Kimerling, J. Michel, E. L. Thomas, Direct-write thermocapillary dewetting of polymer thin films by a laser-induced thermal gradient. *Adv. Mater.* **25**, 6100–6105 (2013).
53. J. P. Singer, K. W. Gotrik, J.-H. Lee, S. E. Kooi, C. A. Ross, E. L. Thomas, Alignment and reordering of a block copolymer by solvent-enhanced thermal laser direct write. *Polymer* **55**, 1875–1882 (2014).
54. K. Negita, Electrorheological effect in the nematic phase of 4-*n*-pentyl-4′-cyanobiphenyl. *J. Chem. Phys.* **105**, 7837–7841 (1996).
55. K. Terao, J. W. Mays, On-line measurement of molecular weight and radius of gyration of polystyrene in a good solvent and in a theta solvent measured with a two-angle light scattering detector. *Eur. Polym. J.* **40**, 1623–1627 (2004).
56. C. B. McArdle, *Side Chain Liquid Crystal Polymers* (Chapman and Hall, 1989).
57. S. Nersisyan, N. Tabiryan, D. M. Steeves, B. R. Kimball, Fabrication of liquid crystal polymer axial waveplates for UV-IR wavelengths. *Opt. Express* **17**, 11926–11934 (2009).
58. H. Sarkissian, S. V. Serak, N. V. Tabiryan, L. B. Glebov, V. Rotar, B. Y. Zeldovich, Polarization-controlled switching between diffraction orders in transverse-periodically aligned nematic liquid crystals. *Opt. Lett.* **31**, 2248–2250 (2006).
59. H. Sarkissian, B. Park, N. Tabirian, B. Zeldovich, Periodically aligned liquid crystal: Potential application for projection displays. *Mol. Cryst. Liq. Cryst.* **451**, 1–19 (2006).
60. H. Zhang, S. Shiino, A. Shishido, A. Kanazawa, O. Tsutsumi, T. Shiono, T. Ikeda, A thiophene liquid crystal as a novel π-conjugated dye for photo-manipulation of molecular alignment. *Adv. Mater.* **12**, 1336–1339 (2000).
61. M. Born, E. Wolf, *Principles of Optics* (Cambridge Univ. Press, 1999).
62. K. Matyjaszewski, Atom transfer radical polymerization (ATRP): Current status and future perspectives. *Macromolecules* **45**, 4015–4039 (2012).
63. P. Jiang, J. F. Bertone, K. S. Hwang, V. L. Colvin, Single-crystal colloidal multilayers of controlled thickness. *Chem. Mater.* **11**, 2132–2140 (1999).
64. P. F. Van Kessel, L. J. Hornbeck, R. E. Meier, M. R. Douglass, A MEMS-based projection display. *Proc. IEEE* **86**, 1687–1704 (1998).

Acknowledgments

Funding: This work was supported by the Precursory Research for Embryonic Science and Technology program, "Molecular Technology and Creation of New Functions" (no. JPMJPR14K9), and the Japan Science and Technology Agency. This work was supported by the Japan Society for the Promotion of Science (JSPS) KAKENHI grant no. JP17H05250 in Scientific Research on Innovative Areas "Photosynergetics." This work was supported by JSPS KAKENHI grant no. JP17J09899. This work was performed under the Cooperative Research Program of "Network Joint Research Center for Materials and Devices." This work was performed under the Research Program for CORE Lab of "Dynamic Alliance for Open Innovation Bridging Human, Environment and Materials" in "Network Joint Research Center for Materials and Devices." **Author contributions:** K.H. and A.S. conceived the project. K.H., M.A., M.I., Y.K., and W.N. performed these sample preparations and characterizations for fabricating molecularly aligned polymer films with various chemical systems and analyzed the alignment patterns. W.N. synthesized the well-defined polymers by ATRP and conducted a test system of diffusion-induced molecular alignment, and K.H. and W.N. analyzed the data and estimated the theoretical model. K.H., N.A., C.J.B., and A.S. designed the optical pattern for arbitrary alignment patterns, and K.H., and Y.K. conducted the experiments. K.H., N.A., C.J.B., and A.S. prepared the manuscript, incorporating contribution from all authors. **Competing interests:** K.H., M.A., and A.S. are authors on several patent applications related to this work registered with the Japan Patent Office (application no. 2013-137132, filed 28 June 2013; application no. 2014-534217, filed 10 June 2013; application no. 2013-176129, filed 27 August 2013; application no. 2016-089011, filed 27 April 2016). The other authors declare that they have no competing interests. **Data and materials availability:** All data needed to evaluate the conclusions in the paper are present in the paper and/or the Supplementary Materials. Additional data related to this paper may be requested from the authors.

Submitted 15 May 2017
Accepted 17 October 2017
Published 10 November 2017
10.1126/sciadv.1701610

Citation: K. Hisano, M. Aizawa, M. Ishizu, Y. Kurata, W. Nakano, N. Akamatsu, C. J. Barrett, A. Shishido, Scanning wave photopolymerization enables dye-free alignment patterning of liquid crystals. *Sci. Adv.* **3**, e1701610 (2017).

ScienceAdvances

Scanning wave photopolymerization enables dye-free alignment patterning of liquid crystals

Kyohei Hisano, Miho Aizawa, Masaki Ishizu, Yosuke Kurata, Wataru Nakano, Norihisa Akamatsu, Christopher J. Barrett and Atsushi Shishido

Sci Adv **3** (11), e1701610.
DOI: 10.1126/sciadv.1701610